RSC Advances

ROYAL SOCIETY OF CHEMISTRY

www.rsc.org/advances

RSC Advances

ARTICLE

Induced Conformational Change on Ferrocenyl-Terminated Alkyls and its Application as a Transducer for a Label-Free Immunosensing of Alzheimer's Disease Biomarker[§]

Received 00th January 20xx,
Accepted 00th January 20xx

DOI: 10.1039/x0xx00000x

www.rsc.org/

Abdelmoneim Mars,[a] Wicem Argoubi,[a] Sami Ben Aoun[b]* and Noureddine Raouafi [a]*

Alzheimer's disease is the second most common neurogenerative illness affecting elderly people. Early diagnostic could help improving the patients' life quality. The classical sandwich ELISA-based methods are usually costly and time consuming. In this study, we report the design of a label-free immunosensing platform for the sensitive detection of ApoE protein as a biomarker of Alzheimer's disease. The immunorecognition event induces conformational changes in ferrocenylalkyl tethered to the superficial gold nanoparticles in the vicinity of the antibody. The heavy antigen/antibody complex enhances the electron-transfer (ET) rate constants by bending the ferrocenylalkyl chain bringing the ferrocene closer to the gold surface. Determination of the ET rate constants and the analytical performance studies for a series of devices using ferrocenylakyl with different chain lengths support the proposed mechanism. The best performances and the highest rate constants are observed with sensors having the most flexible chains. The devices are endowed with a large dynamic range (i.e. 0.13 to >1880 ng.mL^{-1}) and excellent selectivity and specificity.

1. Introduction

Inherently endowed with several interesting features such as selectivity and sensitivity of analysis, high repeatability, easiness of signal quantification, etc.,[1] electrochemical biosensors are in the direct line to produce devices for point-of-care applications since they comply with the basic requirements for such applications.[2] On the another hand, ferrocene derivatives are good candidates to electrochemically transduce biological events and to regenerate redox-active sites in enzymes by acting as electron mediators because of their low oxidation potentials, fast ET rates and stability in aqueous medium.[3] Moreover, ferrocene has been extensively used to study the ET in model systems such as thiol-terminated self-assembled monolayers (SAMs) of alkyl groups or peptides with an end-capping ferrocene group.[4] Also ferrocene has been covalently linked *via* an alkyl spacer to boron-doped diamond electrode.[5] Two major mechanisms have been recognized: (i) for dense self-assembled layers, electrons tend to travel through the carbon-carbon bond from the ferrocene group to reach the electrode surface (tunnelling mechanism)[6] and (ii) electrons migrate by hopping from one site to another especially in proteins.[7] Recently, it has been reported that the ET can be enhanced by conformational disorder or on the contrary can be gated by conformational changes.[5] Changes in the DNA conformation were also exploited to develop a highly sensitive electrochemical hybridization-based DNA sensor through the monitoring of ET from the ferrocene in a favourable position allowing facile ET and another one impeding it.[8]

There are numerous reports on the use of ferrocene in immunosensing of cancer biomarkers. For instance, ferrocene and thionine were covalently conjugated to anti-α-fetoprotein (AFP) and α-carcinoembroyonic antigen (CEA) antibodies, respectively, and co-immobilized on a glassy carbon electrode modified with gold nanoparticles and conjugated with horseradish peroxidase (HRP) to develop a sensitive amperometric immunosensor for simultaneous determination of AFP antigen and CEA.[9] The two antigens can be detected in a single run with the same dynamic range (*i.e.* 0.01-50 ng.mL^{-1}) and the same limit of detection (~0.01 ng.mL^{-1}). CEA was also

[a] University of Tunis El-Manar, Faculty of Science of Tunis, Chemistry Department, Laboratory of Analytical Chemistry and Electrochemistry (LR99ES15), Campus Universitaire de Tunis El-Manar 2092, Tunis, Tunisia. *Corresponding author: Noureddine Raouafi (n.raouafi@fst.rnu.tn), Tel.: +21671872600 (Ext. 273); Fax: +21671883424

[b] Department of Chemistry, Faculty of Science, Taibah University, PO. Box 30002 Al–Madinah Al–Munawarah, Saudi Arabia. *Corresponding author: Sami Ben Aoun (sbenaoun@taibahu.edu.sa), Tel.: +966590900727; Fax: +966148618888 (Ext. 4326)

[§] Electronic Supplementary Information (ESI) available: [organic synthesis of the molecules, electrochemical measurements]. See DOI: 10.1039/x0xx00000x

detected in saliva and serum using an electrochemical ELISA-like immunoassay. CEA has been sandwiched between monoclonal α-CEA antibodies, covalently immobilized on polyethyleneimine-wrapped CNTs casted on screen-printed electrodes, and ferrocene carboxylic-tagged acid α-CEA encapsulated liposomes. The addition of CEA induces an increase of the differential pulse voltammetry (DPV) current proportionally to the antigen amounts.[10] In another report, ferrocene functionalized-peptide nanowires having a diameter of *ca*. 100 nm were synthetized, coated with poly(diallyldimethyl-ammonium chloride), conjugated with antibodies and decorated with gold nanoparticles, then used as a detection probe for an ultrasensitive electrochemical sandwich immunosensor for human IgG. The capture probe was immobilized on a gold nanoparticles/graphene composite.[11]

On the other hand, apolipoprotein E (ApoE) class of proteins are essential to the metabolism of triglyceride-rich lipoproteins and to the central nervous system.[12] Monitoring of these proteins and the presence of ApoE4 isoform has been used as a biomarker for Parkinson's or Alzheimer's diseases.[13] ApoE levels in cerebrospinal fluid (CSF) for Alzheimer's disease (AD) patients are 3-folds higher than control subjects (4.66 ±1.96 µg/mL vs. 1.92 ±1.46 µg/mL).[14] For blood plasma, these levels are 61.50 ±22.04 µg/mL and 52.31 ±16.61 µg/mL respectively for AD patients and healthy persons with the APOE ε4/ε3 genotype.[15] Commonly, ApoE is determined using various immunoassay techniques such as enzyme-linked immunosorbent assay (ELISA), surface Plasmon resonance and other sandwich-like immunoassays.[16] These methods still suffer from several disadvantages like lengthy analysis times, necessity of a second antibody to immunosandwich the antigen, the need for a second antibody labelling and several washing steps. The aforementioned disadvantages can be overcome by a direct immunoassay.

In this paper, we report the direct determination of ApoE using an electrochemical immunosensing platform based on the conformation changes occurring on alkyl chains in ferrocenylalkyl-modified gold nanoparticles as a transducing system during the recognition event. The effects of chain length on the analytical performances and on the ET rate constants have been evaluated using a series of ferrocene derivatives with different chain lengths and ApoE as a model analyte.

2. Experimental

2.1. Materials and reagents

All the chemicals and biochemicals: 1-ferrocenylmethanol (97%), ferrocene carboxylic acid (97%), 2-mercaptoethanol (98%), 4-mercaptobutanol (95%), 8-mercaptooctanol (98%), α-lipoic acid (≥98%), dimethylaminopyridine (DMAP) (99%), dicyclohexylcarbimide (DCC) (99%), glutaraldehyde (GL, 50%), $HAuCl_4.3H_2O$ (99.9%), sodium borohydride (≥98%), human IgG (hIgG, ≥95% from human serum) antibody, ovalbumin (OVA, ≥98%), bovine serum albumin (BSA, 98%), phosphate buffer saline (PBS) in tablet (PBS stands for 0.1 M, pH = 7.4 PBS solutions, unless otherwise stated), silica gel 60 mesh and fluorescent silica-coated aluminium TLC plates were purchased from Sigma-Aldrich (Germany). Chemicals and biochemicals were used without further purification. Capture monoclonal antibody anti-ApoE (α-ApoE produced in vitro cultures) and purified standard ApoE solutions were purchased from Mabtech AB (Nacka Strand, Sweden).

All voltammetric experiments were performed in PBS using a PC-controlled Metrohm Autolab PGSTAT M204 electrochemical workstation with Nova software (v 1.10) for data collection. Screen-printed carbon electrodes (SPCEs) printed on polyethylene terephthalate (PET) sheets with a semi-automatic screen-printing machine (DEK-248, DEK International, Switzerland) were used to perform the electrochemical experiments. The SPCEs comprises of a carbon disk serving as a working electrode (3-mm diameter), a printed Ag/AgCl reference electrode and a carbon wire as a counter-electrode.

Scanning electron microscope (SEM) images were obtained using a field emission SEM (Merlin, CarlZeiss). UV-visible absorption measurements were carried out on a SpectroQuest 2800 spectrophotometer (UNICO, Spain). A thermostatic centrifuge ScanSpeed 1730R (LoboGene A/S, Denmark) was used to purify the AuNP/antibody bioconjugates. All the solutions were prepared in deionized water (>18.2 $M\Omega.cm^{-1}$) produced using Milli-Q system. NMR spectra were recorded in Bruker Advance 300 apparatus in $CDCl_3$ at 300 MHz. Chemical shifts are given in ppm according to tetramethylsilane (TMS) used as an internal reference.

2.2. Preparation of ferrocene derivatives

The ferrocenyl lipoic acid ester (FcL) was prepared according to literature.[17] The FC_nS derivatives (n = 2, 4, 8) were obtained using Steglich conditions according as depicted in Fig. S1 in the Electronic Supporting Information (ESI). Ferrocene carboxylic acid (115.02 mg, 0.50 mmol) and 1.2 equivalent of n-mercapto-1-alcohol (0.60 mmol) were mixed under stirring in dichloromethane at 0 °C for 15 min then 1.2 equivalent of DCC (121.8 mg, 0.60 mmol) and 30% molar of DMAP (18.3 mg, 0.06 mmol) were added. The reaction progress was monitored by TLC. The solution was stirred for 24 hours at room temperature to give the 1-ferrocenyl-n-mercaptoalkyl acid esters (FC_nS) in 65-76% yields. The products were purified by silica column chromatography using ethyl acetate and hexane (3:7). NMR chemical shifts of the products are given in ESI.

2.3. Immunosensor fabrication

The cystamine-capped gold nanoparticles solution were prepared according to a literature procedure.[18] Briefly, 1 mL of a freshly prepared cystamine solution (213.0 mM) was added to 100 mL of tetrachloroauric(III) acid solution (1.42 mM). The mixture turned yellow upon addition of cystamine and was then stirred vigorously for 10 min. After that, a 40 µL of a freshly prepared sodium borohydride solution (10 mM) was quickly injected into the reaction mixture. After vigorous stirring for 20 min, the solution colour turned red-wine. The resulting cystamine-modified gold nanoparticles (cysAuNPs) was stored in the dark at 4 °C.

SPCE was used as substrate and was beforehand cleaned by 25 cyclic voltammetry (CV) runs between -1.5 to +1.5 V in a PBS solution, then thoroughly washed with deionized water. The cysAuNPs-modified electrode was then immediately prepared by drop-casting 5 µL of the cysAuNPs suspension on the working electrode and allowed to dry at room temperature (RT). The surface morphology of the bare and cysAuNPs-modified SPCEs were investigated by SEM, which shows that AuNPs were physically adsorbed on the porous carbon surface, as detailed at the Results and Discussion section. 10 µL of 2.5 mM GL were dropped onto AuNPs modified working electrode area, incubated for 1 hour at 4 °C and washed several times with a PBS solution. The modified electrode was immersed for 3 hours (at 4 °C) into a 100 µg/mL solution of a monoclonal α-ApoE antibodies to covalently immobilize it on the surface then the electrode was washed thoroughly twice with PBS. In the next step, the ferrocene was electrochemically immobilized by dropping 25 µL of 10 mM ferrocene derivative solution on the cysAuNP-modified SPCE and a potential of -0.4 V was applied for 360 seconds (Fig. S2). To avoid any kind of non-specific interactions, the modified electrodes were further immersed in 3% BSA solution for 1h at RT. Finally, the as-prepared immunosensor was washed several times with PBS solution and stored at 4 °C for more than 15 days.

The same experimental procedure was used to immobilize α-ApoE antibodies used for the study of the effect of ferrocene derivative chain lengths on the immunosensing response.

In order to characterize the first modification step of SPCE with AuNPs, cyclic voltammetry was performed by scanning the potential between -0.9 and +1.3 V in 0.5 M H_2SO_4 solution at a scan rate of 0.1 V/s. The stepwise surface modification was monitored by electrochemical impedance spectroscopy (EIS) at an applied potential of 0.2 V. For this, a 50 µL aliquot of a (0.1 M KCl + 5 mM $[Fe(CN)_6]^{4/3-}$) solution was casted on the electrode surface then the frequency was swept from 100 MHz to 0.1 Hz. All the EIS data are presented as Nyquist plots (i.e. the reciprocal of the real component of the impedance plotted against the imaginary one).

2.4. Immunoassay and electrochemical detection

The α-ApoE/FcL/cysAuNPs/SPCE was incubated for 30 min at RT with 50 µL of different concentrations of the ApoE solutions followed by washing with PBS before the electrochemical measurements. For all the immunosensing experiments,

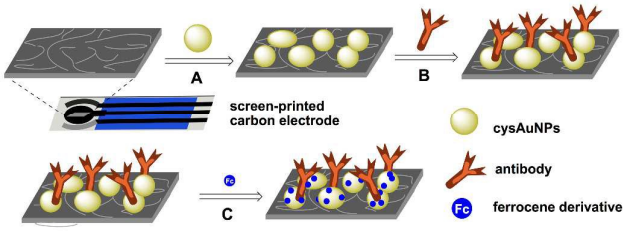

Fig. 1 Schematic representation of the immunosensor preparation: (A) adsorption of the cysAuNPs onto the SCPE surface, (B) biofunctionalization with antibody reticulated by glutaraldehyde and (C) modification by the ferrocene derivative.

differential pulse voltammetry (DPV) curves were recorded at a scan rate of 50 mV/s. The immunosensing event is correlated with the variation in the current response before and after immunoreactions. Therefore, the changes in the current response (Δi) of the immunosensors were evaluated as follows: $\Delta i = i_f - i_i$, where i_i and i_f represent the current response of the immunosensors prior and after the electrode incubation into a given concentration of the antigen, respectively. The same experimental procedure was followed for the α-ApoE/FC_nS/cysAuNPs/SPCE incubation with ApoE, performed to study the effect of the ferrocene derivative chain lengths on the immunosensing response and on the ET rate constants.

Chronoamperometry was used to monitor the ApoE immunosensing. Chronoamperograms were recorded at potentials of 0.31, 0.54, 0.57 and 0.61 V which correspond to the oxidation potentials of the ferrocene derivatives FcL, FC_2S, FC_4S and FC_8S, respectively.

3. Results and discussion

3.1. Immunosensor design

The ApoE immunosensor was fabricated in a straightforward manner through the consecutive modification of the substrate, as schematically outlined in Fig. 1. CysAuNPs were first used to coat the working surface of SPCE. The deposition of cysAuNPs onto bare electrode was confirmed by SEM. A typical rough surface was observed in the case of bare electrode (Fig. 2A), while for the cysAuNPs/SPCE, AuNPs were uniformly dispersed but few aggregated particles on the carbon surface were observed (Fig. 2B). The average diameter of these nanoparticles is ~20 nm.

CV and EIS were used to characterize the electrode surface modification. The different CVs are displayed in Fig. 2C. The inset shows the CV recorded between 0 and 1.5 V for bare and cysAuNP-modified SPCEs in a 0.5 M H_2SO_4 solution. No faradic current was observed for the bare electrode, whereas a typical curve related to the presence of a gold layer was obtained for the modified electrode. Three redox peaks can be observed; two during the forward scan (at *ca*. 0.8 and *ca*. 1.2 V) and one at 0.6 V during the reverse scan corresponding to the oxidation of gold to gold(III) species and their subsequent reduction to gold(0), respectively.[19]

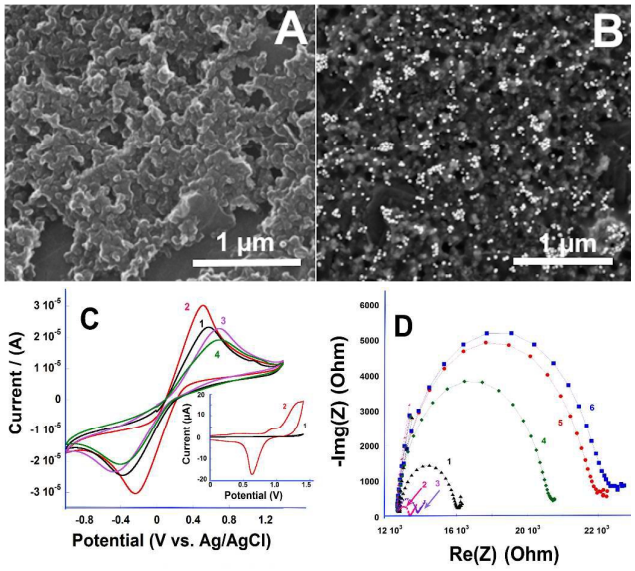

Fig. 2 (A and B): SEM images of the bare SPCE and cysAuNPs-modified SPCE, respectively; CVs (C) and EIS plots (D) of SPCEs performed in 0.1M KCl containing 5 mM $[Fe(CN)_6]^{4/3-}$ after each step of the modification (inset (c): CVs of bare SPCE (black) and cysAuNPs-modified SPCE (red) performed in a 0.5M H_2SO_4 solution at 100 mV/s sweep rate). 1: SPCE, 2: cysAuNPs/SPCE, 3: GL/cysAuNPs/SPCE, 4: FcL/GL/cysAuNPs/SPCE, 5: α-ApoE/FcL/GL/cysAuNPs/SPCE, 6: BSA/α-ApoE/FcL/GL/cysAuNPs/SPCE

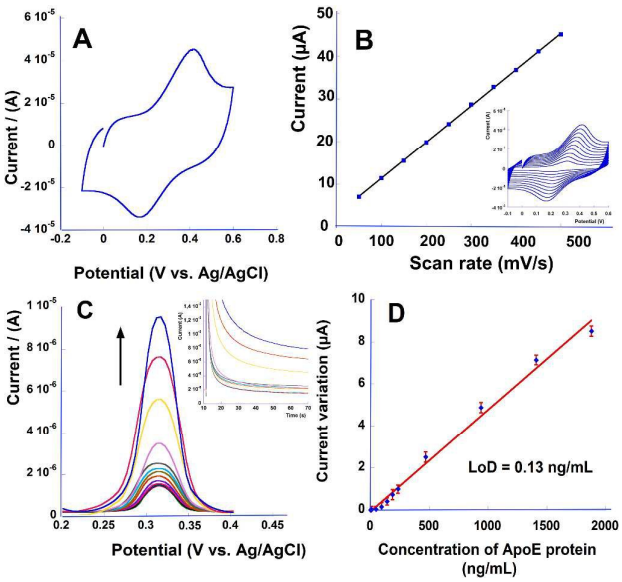

Fig. 3 (A): CV of the α-ApoE/FcL/cysAuNPs/SPCE immunosensor recorded in PBS at 500 mV/s; (B): plot of the current versus the scan rate (ip vs. v) (Inset: CVs of the biosensor recorded in PBS at various scan rates from 50 to 500 mV/s); (C): DPV signal increase evidencing ApoE/anti-ApoE recognition in the biosensor after incubation in different ApoE solutions with gradually increasing concentrations (inset: variation of chronoamperometry current after incubation in the same solutions) and (D): Plot of current increase (Δ*i*) vs. the ApoE amounts and fitting the curve.

Using $[Fe(CN)_6]^{4/3-}$ to probe the surface modification, the potential was scanned between -0.9 and +1.3 V (Fig. 2C). From the figure, we can conclude that a little gain in reversibility and a better ET are obtained after the surface modification with AuNPs, which are partially lost in the subsequent steps because of the introduction of an electronic transfer-impeding layer formed by glutaraldehyde and the antibodies.[20] Furthermore, EIS was used to monitor the immunosensor preparation. Fig. 2D exhibits the Nyquist plots of a series of modified electrodes. It is clearly shown that a relatively large charge-transfer resistance (R_{ct}) was observed at bare SPCE (curve 1) which drastically decreased after the nanostructuration of the surface by cysAuNPs (curve 2) in agreement with previous reports.[21] The immobilization of glutaraldehyde onto cysAuNPs/SPCE was accompanied with a gentle R_{ct} increase (curve 3). This slight increase was perhaps due to the blocking effect of glutaraldehyde.[22] Another prominent increase of the resistance was observed after the introduction of the ferrocene derivative (curve 4). Finally, immobilization of α-ApoE antibody and BSA induces a further increase of the charge-transfer resistance as shown in curves (5) and (6), respectively.

The α-ApoE/FcL/cysAuNPs/SPCE immunosensor displayed a reversible CV signal related to the oxidation of ferrocene moiety to ferrocenium cation as displayed in (Fig. 3A). Moreover, plotting of oxidation and reduction peak currents vs the sweep rate showed a linear relationship suggesting a surface-confined ET process and confirming the immobilization of ferrocene derivative on the electrode surface (Fig. 3B).[23] The 3% of BSA solution were used to cover the gold surface to prevent any kind of non-specific protein interactions.

3.2. Immunosensing of ApoE biomarker

Immunoassays were performed by incubating the as-prepared immunosensors in a series of ApoE solutions prepared at different concentrations; the change in ferrocene oxidation current before and after the incubation was used to monitor the immunoreaction. Immunosensor response to ApoE was preferably calibrated using DPV rather than CV as the former was found more sensitive and reproducible. DPV voltammograms (Fig. 3C) exhibited a gradual increase in Δ*i* values with increasing concentration of ApoE protein in the linear fashion (Cf. Fig. 3D). We speculate that the current variation (Δ*i*) is induced, somehow, by the antigen-antibody immunocomplex formation (*vide infra* for a proposal of the mechanism). For instance, a marked increase in Δ*i* was found to be *ca*. 4.87 µA for an incubation with ≈ 1000 ng/mL ApoE solution.

Plotting the Δ*i* versus ApoE antigen amounts gives a straight line (R = 0.9989) for a large dynamic range (*i.e.* 0.13 to 1880 ng/mL) with a RSD = 4.3%, which confirms the good reproducibility of measurements (Fig. 3D).[24] Based on the correlation graph, the sensitivity of the immunosensor was estimated to be *ca*. 4.37 nA.mL.ng^{-1}. Chronoamperometry was also employed to corroborate the DPV findings. A series of chronoamperograms was recorded at 0.31 V corresponding to the ferrocene oxidation potential with an ApoE concentration range between 0.47 and 1880 ng.mL^{-1} (inset of Fig. 3C). In agreement with the DPV data, the current response of ferrocene oxidation increased linearly with ApoE concentration.

3.3. Optimization of ferrocene chain length and chain anchor

To optimize the chain length of the ferrocene transducer which is immobilized on the immunosensor surface, a series of

different immunosensors using ferrocene derivatives with different chain lengths (i.e. FcL (6C) and FC_nS, with n = 2, 4, 8) were evaluated.

DPV studies (Cf. Figs. S3A, S4A and S5A) revealed that the highest sensitivity of the response of FC_nS-containing biosensors was obtained when the longest carbon chain (*i.e.* FC_8S) was utilized, reaching the value of *ca*. 4.26 nA.mL.ng^{-1}, which dropped by more than 57% for the shortest chain (Fig. 4A). These results were also confirmed by chronoamperometry (Cf. Figs. S3B, S4B and S5B of ESI), revealing a direct relationship between the chain length and the sensing performances (Fig. S6 of ESI).

One plausible explanation of these observations is that the ApoE (34 kDa).[25] addition leads to the formation of a heavy immunocomplex which will bend the alkyl chain and brings the ferrocene moiety closer to the surface.

Furthermore, the importance of the nature of the anchor site (*i.e.* the linker between AuNPs and ferrocene moiety) was also evaluated. Ferrocenyl-8-mercaptooctyl acid ester (FC_8S) and ferrocenyl lipoic acid ester (FcL) were selected for this study. The results shown in Fig. 4B suggest that the use of a disulfide anchor group leads to a more robust and sensitive biosensor, thanks to its two sulfur anchoring groups,[23,26] compared to the one with a single thiol site. In fact, and based on the sensitivity of the electrochemical response of these two ApoE immunosensors, the sensitivity of FcL was found to be *ca*. 5.15 nA.mL.ng^{-1} against *ca*. 4.26 nA.mL.ng^{-1} for FC_8S.

3.4. Performances of the ApoE immunosensor

To evaluate the selectivity and the specificity of ApoE immunosensor, different interfering proteins such as hIgG, gIgG, BSA and OVA were investigated to examine their effect on the immunocomplex formation. Selectivity tests were conducted by measuring the electrochemical response of the immunosensor for *ca*. 100 pg [94 ng/mL] of ApoE antigen and comparing it to that obtained in the presence of interfering proteins. For instance, the incubation of immunosensor in 100 ng.mL^{-1} solution of hIgG revealed no effect on the electrochemical response of the immunosensor while the addition of ca. 100 pg of ApoE induces approximately 25% increase in current as shown in DPV measurements (Fig. 5A). Similar results were obtained with BSA, and gIgG (data not shown). Based on the results summarized in the histogram in Fig. 5B, we conclude that the immunosensor is highly selective for ApoE antigen.

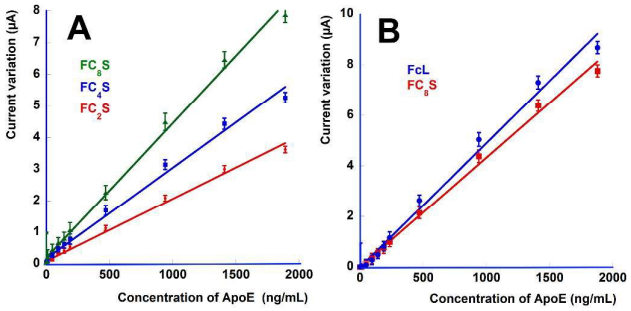

Fig. 4 (A) Increase of DPV current vs. ApoE amounts for the immunosensors prepared using ferrocene derivatives with different chain length: FC_8S (green; 8 carbon atoms), FC_4S (blue; 4 carbon atoms) and FC_2S (red; 2 carbon atoms) and corresponding fitting curves and (B) variation in DPV current vs. ApoE amounts for ApoE immunosensors functionalized with FC_8S (blue) and FcL (red) and correspondent fitting curves.

Table 1 Results of the detection of ApoE in real sample of human blood serum and recovery percentages after successive additions

Detected concentration (P)	Added concentrations (Q)	Detected after addition concentrations (R)	% recovery 100*(R-P)/Q (±std dev.)
58.0	10.0	69.8	105.1±3.4
-	20.0	82.3	107.4±4.2
-	30.0	93.7	109.8±4.7

Additional experiments were performed to ascertain the ApoE immunosensor specificity. The results are summarized in the histogram presented in Fig. 5D. The DPV currents observed as a response to the antigen alone and to the antigen in the presence of a one-thousand-fold of interfering protein (Fig. 5C) show no significant difference (*i.e.* less than 1.1%) which confirms the specificity toward ApoE. Thus, the prepared biosensor can discriminate ApoE in the presence of a large excess of hIgG, BSA, OVA and gIgG. Each measurement performed in this part was run in triplicate to ensure the reproducibility of response.

Since the levels of ApoE in human serum are in the µg per millilitre range,[14-15] the sample was diluted 1:5000 in order to meet the linear range of the reported ApoE immunosensor. The ApoE concentrations were measured and the obtained

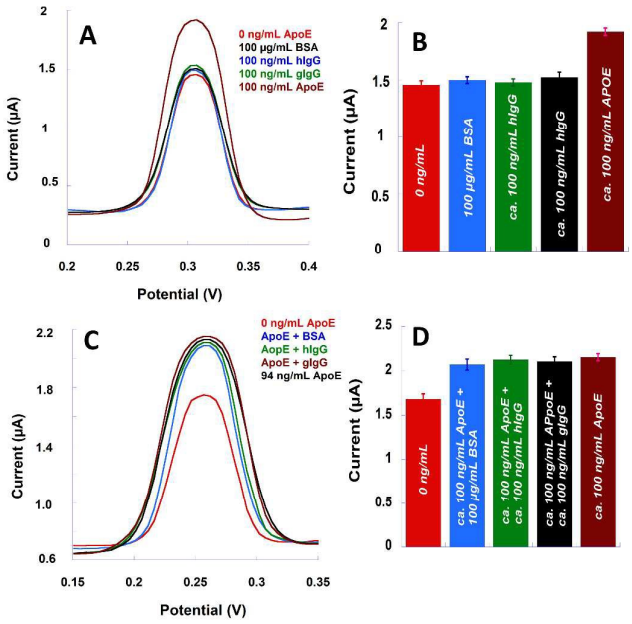

Fig. 5. (A): DPV measurements for selectivity and specificity tests of ApoE immunosensor in presence of hIgG, BSA and gIgG as interfering proteins; (B): selectivity for ApoE; (C): histogram summarizing the current response observed for selectivity test; DPVs performed during the specificity study and (D): summary of results for the specificity test.

data are summarized in Table 1. After that, 10, 20 and 30 ng. mL^{-1} amounts of ApoE protein were injected in the solution and the final concentrations were measured a second time (Fig. S7). The resulted high recovery values 105.1-109.8% with a standard deviation less than 4.7% indicate the good performance of the developed ApoE immunosensor.

Furthermore, the as-obtained ApoE immunosensor results were compared with those of other immunoassay biosensing systems developed to monitor the levels of ApoE protein (Table 2). Table 2 summarizes the detection limits, concentration ranges, analysis time and linear slope of ApoE with other various detecting methods such as CV, square wave voltammetry (SWV), ELISA and SPR. The current method exhibits a great potential for ApoE sensing with a rapid analysis time compared to ELISA method. In addition, a wider linear concentration range and a lower limit of detection compared to other techniques. It has also a high sensitivity as expected by the slope value of the calibration curve.

3.5. Mechanism of the immunosensing response

We speculated that the aforementioned increases in ferrocene oxidation currents during immunoreaction could be ascribed to the antigen/antibody complex formation. Hypothetically, the immunocomplex exerts a mechanical pressure on the ferrocene transducer to induce conformational changes in the alkyl chain bearing the end-capping ferrocene group. As it was pointed out earlier, the ET rate constants from ferrocene group covalently immobilized on conductive surfaces are strongly dependent on the surface coverage and the conformational changes.[5] In this scenario, the alkyl-terminated ferrocene moiety will bend to bring the ferrocene closer to the surface which will allow the electron to hope which, in turn, will cause current increases as illustrated in Fig. 6. Conversely, if the electrons travel to the electrode through a tunnelling mechanism the ET rate should drop with the chain length increase.

To demonstrate this hypothesis, the series of ApoE immunosensors prepared previously were evaluated. For instance, the rate constants (k_{ET}) for ET between the redox centres and the surface were determined using Laviron approximation based on Bulter-Volmer theory and the experimental measurements of the overpotential.[‡4,33] CV curves of the immunosensors in the presence of different ApoE concentrations were recorded at scan rates ranging from 200 to 4000 $mV.s^{-1}$ (inset of Fig. 6B). The extracted values of k_{ET} from the plots of the $\Delta E_p = E_{1/2}-E_p$ (E_p is the anodic or cathodic peak potentials and $E_{1/2} = (E_{pa} + E_{pc})/2$) as function of the logarithm of scan rates (Fig. 6B) are summarized in Table 3. From this table, one can easily notice that the k_{ET} increases with increasing alkyl chain length bearing the ferrocene, as well as with the analyte concentration. For instance, the more flexible chain shows larger increases in k_{ET} as compared to the shorter ones (*i.e.* 0.63×10^3 s^{-1} *vs.* 0.45×10^3 s^{-1} and 0.18×10^3 s^{-1} from C_8 to C_2, C_8 to C_4 and C_4 to C_2, respectively) as estimated when 188 ng/mL of the analyte is added to the biosensors. These facts suggest that the chain flexibility and the mechanical strain exerted by the antigen are governing the ET hopping from the ferrocene to the electrode surface. These findings support our proposed mechanism of the immunosensing response since the aforementioned results

Table 2 Summary of works reporting ApoE immunosensing systems (MBs: magnetic beads, CM: cellulose membrane, GCE: glassy carbon electrode, CA: chronoamperometry, HER: hydrogen evolution reaction, WOR: water oxidation reaction, QDs: quantum dots, IrO_2NPs: iridium oxide nanoparticles, ITO: indium-doped tin oxide, fracAu: fractal gold nanostructures, ALP: alkalin phosphatase, FL: fluorescence, NA: non-available, Bt: butin, Avi: Avidin).

Designed Biosensor	Range ($ng.mL^{-1}$)	LoD ($ng.mL^{-1}$)	Time of analysis (hours)	Detection technique	Ref.
CM/αApoE/ApoE/α-ApoE/ALP	50-1000	0.04	24 h (overnight)	Amperometric / p-AP oxidation	16c
ITO/fracAu/α-ApoE/ApoE/α-ApoE/HRP	1-1000	0.30	5 h	CV	25
MBs/α-ApoE/ApoE/α-ApoE/IrO_2NPs	100-1000	68	15 h (overnight)	CA / WOR	27
MBs/αApoE/ApoE/ αApoE-Bt/Avi-CdSe@ZnS QDs	10-200	12.5	14 h (overnight)	SWV / QDs detection	28
MBs/α-ApoE/ApoE/α-ApoE/AuNPs	0.1-12.5	0.080	14 h (overnight)	CA / HER	29
ELISA plate/αApoE/ApoE/ αApoE-Bt/Avi-CdSe@ZnS QDs	-	0.062	16 h (overnight)	ELISA/FL	30
ELISA plate/ApoE/PBS/αApoE/gIgG/ALP	25-200	-	17 h (overnight)	ELISA	31
ELISA plate/α-ApoE/ApoE/α-ApoE/β-galactosidase	NA	NA	13 h (overnight)	ELISA	32
ELISA plate/α-ApoE/ApoE/α-ApoE/HRP	NA	NA	17 h (overnight)	ELISA	14
SPCE/AuNPs/FcL/α-ApoE/ApoE	0.47- 1800	0.13	5 h	DPV	this work

regarding the improvement of ET rate constants with increasing ferrocenylalkyl chain length differ from the case of ET by tunnelling mechanism where the k_{ET} should proportionally decrease with the increasing of chain length.[4]

Table 3 Values of k_{ET} determined for the alkyl-terminated ferrocene biosensors in presence of different concentrations of ApoE.

[ApoE4] / ng.mL^{-1}	k_{ET} (FC_2S) / s^{-1}	k_{ET} (FC_4S) / s^{-1}	k_{ET} (FC_8S) / s^{-1}
0	3.64 x 10^3	3.75 x 10^3	3.79 x 10^3
94	3.71 x 10^3	3.84 x 10^3	4.16 x 10^3
188	4.13 x 10^3	4.31 x 10^3	4.76 x 10^3

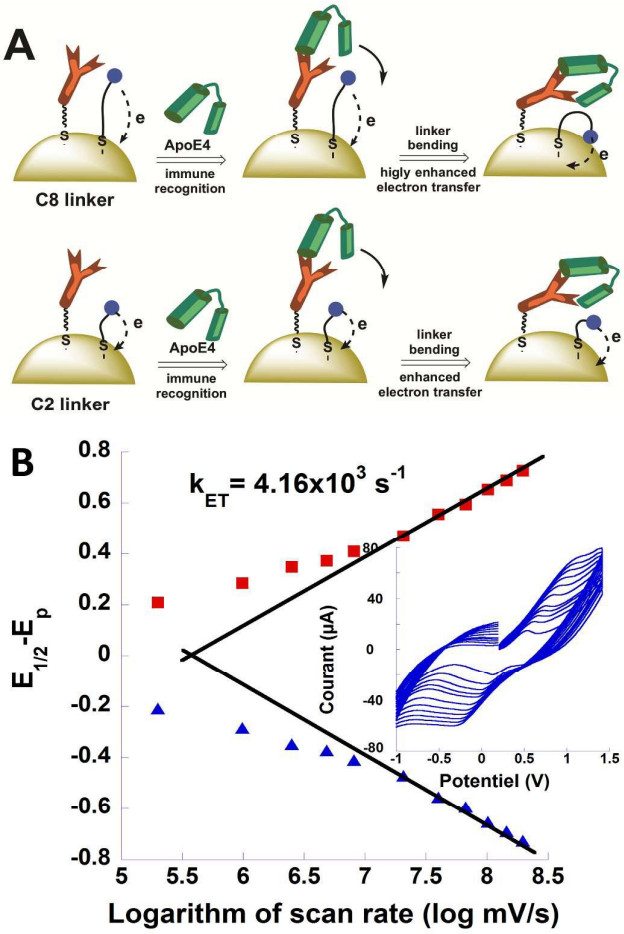

Fig. 6 (A) As-proposed mechanism explaining the current increase during the immunocomplex formation for the two biosensors having ferrocene long and short linkers to the gold and (B) the variation plot of the difference E_p-$E_{1/2}$ as a function of the logarithm of scan rate. Inset: Cyclic voltammograms of FC_8S-based immunosensor in the presence of 94 ng.mL^{-1} of ApoE.

4. Conclusion

In this work, we presented a novel platform for the direct immunosensing of ApoE protein. The label-free platform uses ferrocene covalently immobilized on α-ApoE/cysAuNPs on SPCE. The novelty in the concept is that the immunosensing event induces conformational changes in the alkyl chain, which increases ferrocene oxidation current through the electron hopping from the ferrocene moiety to the electrode surface. The proposed mechanism was assessed by measuring the effect of the chain length and the ET rate constants on the immunosensor performances. The ApoE sensor exhibits a large dynamic range with a high sensitivity and a good detection limit of *ca*. 0.13 ng.mL^{-1}.

Acknowledgements

The University of Tunis El-Manar and the Laboratory of Analytical Chemistry and Electrochemistry (LR99ES15) are gratefully acknowledged for the financial support and the mobility grants awarded to AMM and WA through the "Bourses d'Alternance" program.

Notes and references

‡ Detailed equations for the determination of k_s using Laviron method's and others can be found in the review by Eckermann et al. (ref. 4).

1 D. Tang, B. Su, J. Tang, J. Ren, G. Chen, *Anal. Chem*., 2010, **82**, 1527; N. Ronkainen, J. Thomas, B. Halsall, W. Heineman, *Trends Anal. Chem*., 2002, **21**, 213; M. Dequaire, C. Degrand, B. Limoges, *Anal. Chem*., 2000, **72**, 5521; L. Nyholm, *Analyst*, 2005, **130**, 599; S. Arya, S. Singh, B. Malhotra, *Handbook of Biosensors and Biochips*, Wiley & Sons, Chichester, 2007.

2 D. Lu, J. Wang, L. Wang, D. Du, C. Timchalk, R. Barry, Y. Lin, *Adv. Funct. Mater*., 2011, **21**, 4371; S. Choi, M. Goryll, L. Sin, P. Wong, J. Chae, *Microfluid. Nanofluid*., 2011, **10**, 231.

3 G. Wang, X. Gang, X. Zhou, G. Zhang, H. Huang, X. Zhang, L. Wang, *Talanta*, 2013, **103**, 75; H. Li, Q. Wei, J. He, T. Li, Y. Zhao, Y. Cai, B. Du, Z. Qian, M. Yang, *Biosens. Bioelectron*., 2011, **26**, 3590; S. Kwon, H. Yang, K. Jo, J. Kwak, *Analyst*, 2008, **133**, 1599; S. Dong, B. Wang, B. Liu, *Biosens. Bioelectron.*, 1992, **7**, 215; A. Garcia, C. Peniche-Covas, B. Chico, B. Simpson, R. Villalonga, *Macromol. Biosci*., 2007, **7**, 435.

4 A. Eckermann, D. Feld, J. Shaw, T. Meade, *Coord. Chem. Rev.*, 2010, **254**, 1769.

5 R. Ruther, Q. Cui, R. Hamers, *J. Am. Chem. Soc*., 2013, **135**, 5751.

6 K. Takeda, T. Morita, S. Kimura, *J. Phys. Chem. B*, 2008, **112**, 12840.

7 J. Warren, M. Ener, A. Vlcek, J. Winkler, H. Gray, *Coord. Chem. Rev*., 2012, **25**, 2478.

8 C. Fan, K. W. Plaxco, A. Heeger, *Proc. Natl. Acad. Sci. USA*, 2003, **100**, 9134; F. Ricci, A. J. Bonham, A. C. Mason, N. O. Reich, K. W. Plaxco, *Anal. Chem*., 2009, **81**, 1608; K. J. Cash, F. Ricci, K. W. Plaxco, *J. Am. Chem. Soc.,* 2009, **131**, 6955; K. J. Cash, F. Ricci, K. W. Plaxco, *Chem. Commun.* 2009, 6222; A. Patterson, F. Caprio, A. Vallée-Bélisle, D. Moscone, K. W. Plaxco, G. Palleschi, F. Ricci, *Anal Chem.* 2010, **82**, 9109.

9 W. Lai, J. Zhuang, J. Tang, G. Chen, D. Tang, *Microchim. Acta*, 2012, **178**, 357.

10 S. Viswanathan, C. Rani, A. Anand, J. Ho, *Biosens. Bioelectron*., 2009, **24**, 1984.

11 Y. Ding, D. Li, B. Li, K. Zhao, W. Du, J. Zheng, M. Yang, *Biosens. Bioelectron*., 2013, **48**, 281.

12 X. Han, *Cell. Mol. Life Sci*., 2004, **61**, 1896.

13 M. Takeda, R. Martrinez, T. Kudo, T. Tanaka, M. Okochi, S. Tagami, T. Morihara, R. Hashimoto, R. Cacabelos, *Psych. Clin. Neurosci*., 2010, **64**, 592; J. Kim, J. Basak, D. Holtzman, *Neuron*, 2009, **63**, 287.

14 M. Lindh, M. Blomberg, M. Jensen, H. Basun, L. Lannfelt, B. Engvall, H. Sharnagel, W. Marz, L. Wahlund, R. Cowburn, *Neurosci. Lett*., 1997**, 229**, 85.
15 H. D. Soares, W. Z. Potter, E. Pickering, M. Kuhn, F. W. Immermann, D. M. Shera, M. Ferm, R. A. Dean, A. G. Simon, F. Swenson, G. A. Siuciak, G. Kaplow, M. Thambisetty, P. Zagouras, W. G. Koroshetz, H. I. Wan, G. Q. Trojanowski, L. M. Shaw, *Arch. Neurol*., 2012, **69**, 1310; C. Wang, J. -T. Yu, H.-F. Wang, T. Jiang, C. -C Tan, X.-F. Ming, H. D. Soares, *PLOS One*, 2014, **9**, e89041.
16 M. Porsch-Ozeurumez, S. Westphal, C. Luley, *Clin. Chem*., 2001, **47**, 594; K. Gaus, A. Hall, *Anal. Chem*., 1999, **71**, 2459; M. Meusel, R. Renneberg, F. Spencer, *Biosens. Bioelectron.*, 1995, **10**, 577.
17 A. Mars, C. Parolo, N. Raouafi, K. Boujlel, A. Merkoçi, *J. Mater. Chem. B*, 2013, **1**, 2951.
18 S. Svarovsky, M. Gonzalez-Moa, M. Robida, A. Borovkov, K. Sykes, *Mol. Pharm*., 2009, **6**, 1927.
19 W. Argoubi, M. Saadaoui, S. Ben Aoun, N. Raouafi, *Beilstein J. Nanotechnol*., 2015, **6**, 1840.
20 M. Alonso, C. Yardimci, O. Renedo, M. Martinez, *Anal. Chim. Acta*, 2009, **633**, 51.
21 J. Qui, H. Huang, R. Liang, *Microchim. Acta*, 2011, **174**, 97; G. Jie, B. Liu, H. Pan, J. Zhu, H. Chen, *Anal. Chem*., 2007, **79**, 5574.
22 I. Suni, *Trends Anal. Chem*., 2008, **27**, 604.
23 R. Sahli, C. Fave, N. Raouafi, K. Boujlel, B. Limoges, B. Schollhörn, *Langmuir*, 2013, **29**, 5360.
24 P. De Bièvre, H. Günzler, Validation in Chemical Measurements. Springer, Berlin, 2005.
25 Y. Liu, L.-P. Xu, S Wang, W. Yang, Y. Wen, X. Zhang, *Biosens. Bioelectron*., 2015, **71**, 396.
26 S. Chon, W. Paik, *Phys. Chem. Chem. Phys.*, 2001, **13**, 3405 ; W. Paik, S. Eu, K. Lee, S. Chon, M. Kim, *Langmuir*, 2000, **16**, 10198.
27 L. Rivas, A. de la Escosura-Muñiz, J. Pons, A. Merkoçi, *Electroanalysis*, 2014, **26**, 1287.
28 M. Medina-Sanchez, S. Miserere, E. Morales, A. Merkoçi, *Biosens. Bioelectron*., 2014, **54**, 279.
29 A. de la Escosura-Muñiz, Z. Plichta, D. Horak, A. Merkoçi, *Biosens. Bioelectron*., 2015, **67**, 162.
30 E. Morales-Narváez, H. Montón, A. Fomicheva, A. Merkoçi, *Anal. Chem*., 2012, **84**, 6821.
31 C. Hesse, H. Larsson, P. Fredman, L. Minthon, N. Andreassen, P. Davidsson, K. Blennow, *Neurochem. Res.*, 2000, **25**, 511.
32 H. Song, K. Saito, M. Seishima, A. Noma, K. Unahami, K. Nakashima, *Neurosci. Lett.,* 1997, **23**, 175.
33 E. Laviron, *J. Electranal. Chem. Interfac. Electrochem*., 1979, **101**, 19-28; G. Lenaz, R. Fato, *J. Bioenerg. Biomembranes*, 1986, **18**, 369.

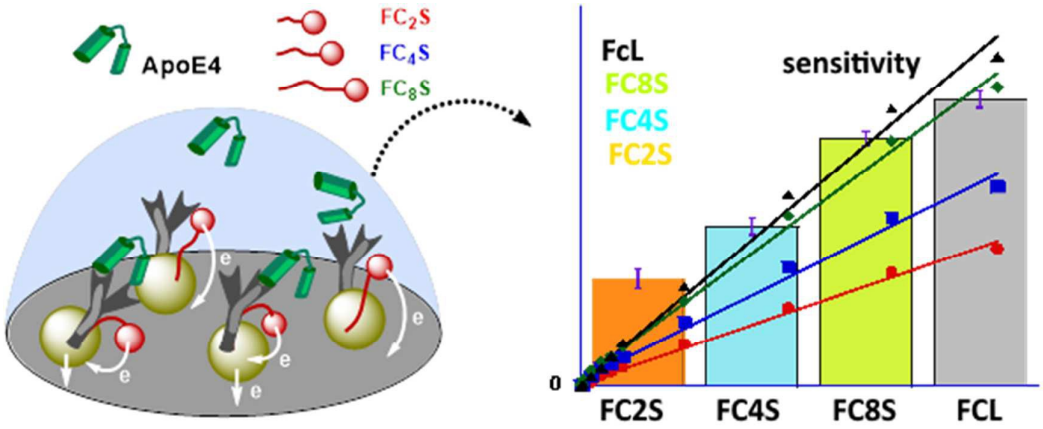

ApoE Alzhzeimer's disease biomarker can be sensitively detected using a label-free platform of flexible ferrocene-terminated alkylchains immobilised on α-ApoE/cysAuNPs/SPCE. The immunorecognition triggers conformational changes which improve the rate constants of electron-transfer